Journal of Biomedical Materials Research Part B: Applied Biomaterials

WILEY

Society For Biomaterials

RESEARCH ARTICLE OPEN ACCESS

Development and Evaluation of the Physico-Chemical and Biological Properties of New Experimental Hydraulic Silicates

Bernardo Almeida Aguiar[1,2] | Anderson Valério Cháves[3] | Marcelo Antônio Santos da Silva[4] | Luiz Thiago Vasconcelos da Silva[5] | Ronaldo Ferreira do Nascimento[5] | Antonio Sérgio Bezerra Sombra[4] | Paulo Goberlânio Barros Silva[1] | Pierre Basílio Almeida Fechine[2] | Marco Antônio Húngaro Duarte[6] | Bruno Carvalho de Vasconcelos[1]

[1]Post-Graduate Program in Dentistry, Faculty of Pharmacy, Dentistry and Nursing, Federal University of Ceará, Campus Do Porangabuçu, Fortaleza, Ceará, Brazil | [2]School of Dentistry, University of Fortaleza, Fortaleza, Ceará, Brazil | [3]Group of Chemistry of Advanced Materials (GQMat), Department of Analytical Chemistry and Physical-Chemistry, Federal University of Ceará, Campus do Pici, Fortaleza, Ceará, Brazil | [4]Telecommunications and Materials Science and Engineering Laboratory (LOCEM), Department of Physics, Federal University of Ceará, Campus do Pici, Fortaleza, Ceará, Brazil | [5]Trace Analysis Laboratory, Department of Analytical Chemistry and Physical Chemistry, Federal University of Ceará, Campus do Pici, Fortaleza, Ceará, Brazil | [6]Department of Dentistry, Endodontics and Dental Materials, Bauru Dental School, University of São Paulo, Bauru, São Paulo, Brazil

Correspondence: Bruno Carvalho de Vasconcelos (bcv@ufc.br)

Received: 17 March 2025 | **Revised:** 29 October 2025 | **Accepted:** 9 February 2026

Keywords: biocompatibility | endodontics | hydraulic cements | physico-chemical properties

ABSTRACT

To evaluate the physico-chemical and biological properties of experimental hydraulic cements (EHCs) prepared after the synthesis of tricalcium silicate (C_3S), calcium zirconium silicate (CZS), and strontium phosphate silicate (SPS) in comparison with Biodentine (BD). After synthesizing and characterizing the silicates (FTIR/XRD/SEM-EDS/TEM), EHCs were analyzed for setting, radiopacity, dimensional stability, compressive strength, solubility, pH, calcium/strontium ion release, and biocompatibility. Significant differences were observed in setting times, with BD<C_3S/CZS and BD/SPS<C_3S, both in initial and final ($p < 0.05$); BD offered shorter times. Regarding radiopacity, the materials ranked as SPS>CZS>C_3S>BD ($p < 0.05$). No differences were observed in dimensional stability (24 h/30 days) ($p > 0.05$). BD showed higher compressive strength than EHCs in both assessed periods ($p < 0.05$); EHCs exhibited an increase over time ($p < 0.05$). Regarding solubility, BD had less mass loss in both periods ($p < 0.05$). Regarding pH, differences were found at 3 h/15 days between BD (8.70; 7.99) and C_3S/CZS cements ($p < 0.05$). At 72 h/168 h, C_3S (9.50; 9.23) showed higher values than SPS/BD and CZS/BD, respectively ($p < 0.05$). For calcium/strontium release, differences were observed at 3 h between C_3S/CZS/BD and SPS ($p < 0.05$). In subsequent periods, SPS provided the highest release, superior to C_3S/CZS ($p < 0.05$). Regarding biocompatibility, no significant differences were observed in the presence of polymorphonuclear cells, mononuclear cells, or fibroblasts ($p > 0.05$); less vascularization was observed at 30 days for BD/C_3S/CZS ($p < 0.05$). Under the study's conditions, it can be concluded that EHCs exhibited promising physicochemical properties, which can still be improved, and adequate biocompatibility. Thus, this article highlights the possibility of developing new silicate-based hydraulic cements.

1 | Introduction

In the search for materials that repair damaged dental structures, ProRoot MTA (Dentsply-Tulsa Dental, Tulsa, OK, USA) was developed in the 1990s [1]. This material contains Portland cement as its major constituent, which includes tricalcium silicate, dicalcium silicate, tricalcium aluminate, and tetracalcium aluminoferrite as primary elements. Although MTA-based cements are recognized for their physico-chemical properties [2, 3], they still have numerous deficiencies, including manipulation and insertion difficulties, long setting times, potential tooth discoloration, and high costs [2, 4].

As an alternative to MTA-based cements, Biodentine (BD; Septodont, Saint-Maur-des-Fossés, France) was introduced. This bioceramic material is developed based on tricalcium and dicalcium silicates, with the addition of calcium carbonate and iron and zirconium oxides in its composition, the latter added as a radiopacifier [5, 6]. Its liquid consists of water, calcium chloride, and a water-soluble polymer. This cement is easy to handle, has high viscosity, short setting times [7]; color stability [7], and biocompatibility [8]. Despite these advantages, BD still has reduced radiopacity [9], cannot be fractionated [10], and requires a mechanical capsule mixer. Additionally, cost may limit its widespread use [11].

New variations in the composition of bioceramics can be formulated, with strontium (Sr) being one of the proposed elements, which acts similarly to calcium (Ca) in bone. A series of in vitro and in vivo studies have demonstrated that strontium ranelate, a medication developed for treating osteoporosis, could stimulate osteogenesis by inhibiting bone resorption [12, 13]. Previous study confirmed that osseointegration could be significantly enhanced by the partial replacement of Ca with Sr. in apatite-based bone cement [14]. Furthermore, strontium exhibits intrinsic radiopacity characteristics, which can help differentiate it from the mineral structures of the body during the repair process [14]. However, its use as an endodontic repair material has not yet been suggested.

Despite the undeniable advancements in bioceramics used for endodontic repair, these materials still have limitations that could be improved by developing new bioactive materials, possibly including new substances. Considering this, the objective of the present study was to synthesize three silicates: tricalcium silicate (Ca_3SiO_5, C_3S), calcium zirconium silicate ($Ca_3ZrSi_2O_9$, CZS), and strontium phosphate silicate ($Sr_5(PO_4)_2SiO_4$, SPS), characterizing them and evaluating their physicochemical properties such as setting time, radiopacity, dimensional stability, compressive strength, solubility, pH, and calcium ion release capacity, as well as the biocompatibility of experimental hydraulic cements (EHCs) prepared with these materials. Additionally, a comparison was made with the commercial cement Biodentine (BD). The null hypothesis proposed that no significant differences would be observed among the experimental cements and between them and the commercial material.

2 | Materials and Methods

For the study, it was necessary to synthesize the silicates, namely: tricalcium silicate (Ca_3SiO_5) and calcium zirconium silicate ($Ca_3ZrSi_2O_9$), synthesized via solid-state method, and strontium phosphate silicate ($Sr_5(PO_4)_2SiO_4$), synthesized via sol–gel. BD was included as a control group and standard material as previously described.

2.1 | Synthesis of Tricalcium Silicate—C_3S

Calcium oxalate (CaC_2O_4) was prepared through an aqueous reaction between dihydrate calcium chloride ($CaCl_2.2H_2O$) and sodium oxalate ($Na_2C_2O_4$; SYNTH, Sigma-Aldrich) in a molar ratio of 1:1. After the reaction, the resulting precipitate was filtered to separate it from the solution. The material retained on the filter (CaC_2O_4) was dried at 80°C for 24 h to remove moisture. Next, silicon dioxide (SiO_2; Sigma-Aldrich) and calcium oxalate were placed in a mortar. These components were thoroughly homogenized to obtain a uniform mixture. The mixture was then subjected to sintering in a resistive furnace in an oxidative atmosphere at 1400°C for 8 h (5°C/min) [15].

2.2 | Synthesis of Calcium Zirconium Silicate—CZS

For the preparation of CZS, a stoichiometric mixture of calcium oxide (CaO; Sigma-Aldrich), zirconium dioxide (ZrO_2; Sigma-Aldrich), and silicon dioxide (SiO_2; Sigma-Aldrich) was used, following the ratio (% m/m): 40.9, 29.9, and 29.2, respectively. After homogenization, the obtained powder was transformed into discs by uniaxial pressing at 4 MPa and sintered at 1400°C for 6 h (10°C/min) [16].

2.3 | Synthesis of Strontium Phosphate Silicate—SPS

For the preparation of SPS via the sol–gel route, tetraethyl orthosilicate (TEOS; Sigma-Aldrich), ammonium dihydrogen phosphate ($NH_4H_2PO_4$; Sigma-Aldrich), and strontium nitrate ($Sr(NO_3)_2$; Sigma-Aldrich) were used in the molar ratio of 1:2:5, respectively. TEOS was completely hydrolyzed in a mixture of ethanol and deionized water (v:v = 2:1), using nitric acid (HNO_3; Sigma-Aldrich) as a catalyst, under magnetic stirring for 1 h each. Subsequently, a stoichiometric mixture of $NH_4H_2PO_4$ and $Sr.(NO_3)_2$ was added under magnetic stirring at room temperature for 3 h to the already hydrolyzed TEOS solution. After homogenization, the mixture was aged at 60°C for 3 days for gelation and then at 120°C for 5 days. Calcination occurred at 1400°C for 8 h [17].

2.4 | Characterization of Synthesized Silicates

2.4.1 | Fourier Transform Infrared Spectroscopy

Fourier transform infrared spectroscopy (FTIR) data were obtained using a Perkin-Elmer 2000 spectrophotometer (PerkinElmer do Brasil Ltda, São Paulo, SP, Brazil) with a wavelength range of 4000–400 cm^{-1}. Each sample was dried beforehand to remove any moisture and dispersed in KBr (Auros Química Ltda, São Paulo, SP, Brazil) in a 1:10 (w/w) ratio and molded into translucent pellets.

2.4.2 | X-Ray Diffraction

X-ray diffraction (XRD) was performed at room temperature using a Bruker diffractometer (D8 Advance; Bruker do Brasil Ltda, Atibaia, SP, Brazil) with a CuKα tube ($\lambda = 1.5418$ Å), equipped with a LynxEye linear detector: 40 kV voltage and 40 mA current over a scanning range of $2\theta = 5°–80°$ with a measurement increment of 0.02°. The crystalline phase was examined by comparing the pattern with ICSD 24625 (C_3S), ICSD 79453 (CZS), and ICSD 02855 (SPS).

2.4.3 | Scanning Electron Microscopy and Energy Dispersive Spectroscopy

To obtain images via scanning electron microscopy (SEM), a QUANTA 450 FEG microscope (FEI, Amsterdam, Netherlands) was used in conjunction with energy dispersive spectroscopy (EDS). Samples were fixed on carbon tape and metallized with metallic silver using metallization equipment (QT150TES; Quorum Technologies Ltd., Laughton, England). An incident electron beam of 20 kV was applied for image generation.

2.4.4 | Transmission Electron Microscopy

Tansmission electron microscopy (TEM) images of the samples were obtained using a Hitachi HT7700 TEM system (Hitachi High Technologies America Inc., Schaumburg, IL, USA) operating at an acceleration voltage of 120 kV. The samples were initially dispersed in an organic solvent, hexane ($CH_3(CH_2)4CH_3$; Sigma-Aldrich), and deposited on a sample holder made of carbon-coated copper grids. The samples were then dried at 60°C overnight. Images were analyzed using the MB-Ruler 5.2 program (Informer Technologies Inc., Los Angeles, CA, USA) to determine the average particle sizes. A total of 99 measurements for each material were taken, divided into 33 measurements for each captured image. To achieve better homogenization, the 99 measurements were divided into 33 for small grains, 33 for medium, and 33 for large based on a comparative visual estimation [15].

2.5 | Physico-Chemical Tests

With the synthesized and characterized silicates in hand, EHCs were prepared by adding zirconium oxide (ZrO_2; Sigma-Aldrich), included as a radiopacifier in a ratio of 60/40 (w/w). For manipulation, a liquid was prepared by mixing distilled water (SSPLUS do Brasil Ltda, Maringá, PR, Brazil) and polyethylene glycol 1400 (Sigma-Aldrich) in a ratio of 70/30 (v/v). With the liquid prepared, the cements were mixed as powder/liquid in a ratio of 10/3 (w/w) for C_3S and 10/2 (w/w) for CZS and SPS; they were then spatulated until a homogeneous mass was obtained (approximately 40s). The powder/liquid ratio of each EHC was determined through a preliminary flow study based on the ISO 6876/2012 [18] standard, where its flow was standardized to closely approximate that of BD; this was prepared following the manufacturer's recommendations.

The physico-chemical properties of the EHCs and BD were evaluated according to the tests described below.

2.5.1 | Setting Time, Radiopacity, Dimensional Stability, Compressive Strength, and Solubility

The determination of setting time (min.) followed the parameters established in ASTM C266/2008. Radiopacity (mm Al) was determined following the recommendations of ISO 6876/2012 [18]. Dimensional stability (%), compressive strength (MPa), and solubility (%) were also assessed following ISO 6876/2012, with adaptations suggested by Carvalho-Junior et al. and Bernardi et al. [19, 20].

2.5.2 | pH and Calcium/Strontium Release

To analyze pH and the release of calcium/strontium ions, polyethylene tubes ($n = 10$) with a diameter of 1.0 mm and a height of 10 mm, sealed on one side, were filled with the freshly prepared materials. The tubes were then immediately immersed in glass vials, previously treated with nitric acid, containing 10 mL of deionized water, with a pre-measured pH of 6.73 (Asfer Ind. Quim. São Caetano do Sul, SP, Brazil). The vials were placed in an incubator at 37°C and 95% ± 5% relative humidity for periods of 3, 24, 72, 168 h, 15 days, and 30 days. At the end of each period, the polyethylene tubes containing the materials were gently removed and immersed in new vials.

For pH determination, the vials containing the polyethylene tubes were mechanically agitated, and the pH of the liquid was analyzed using a digital pH meter (Model #371; Micronal, São Paulo, SP, Brazil) calibrated with control solutions.

The presence of calcium and strontium ions in the liquid was assessed using flame atomic absorption spectroscopy (SpectraAA 220 FS; VARIAN, NJ, USA). For Ca^{2+} evaluation, a solution of lanthanum nitrate, $La(NO_3)_3$, at a concentration of 10 g/L was used to eliminate interference from phosphates and sulfates, as well as to prevent the possible formation of refractory oxides. The conditions for using the equipment were established according to the manufacturer's recommendations, using a wavelength of 422.7 nm, a slit width of 0.2 mm, a current of 10 mA, and a slightly reducing stoichiometry maintained by an acetylene flow of 2.0 L/min supported by compressed air [21]. For Sr^{2+} evaluation, a flame composed of a mixture of acetylene gas and compressed air was used; the equipment was adjusted to operate at a wavelength of 460.7 nm, with a slit width of 0.5 mm to identify the absorption of Sr. metal. To avoid spectral interference in the determination of Sr^{2+}, KCl at 2000 mg/L was added as an ionization suppressor and $LaCl_3$ at 1% as a releasing agent [22].

2.6 | Biocompatibilty Test

After approval from the Animal Research Ethics Committee (#2539080422), 72 male albino Wistar rats, aged 3–4 months and weighing between 180 and 250 g, were divided into three groups

based on the experimental periods of 15, 30, and 60 days, with 24 animals per period. They were housed in rooms with controlled temperature (21°C to 25°C) and provided with solid food and access to water *ad libitum* before and throughout the experimental period, in an environment with a light cycle of 12 h of light and 12 h of darkness.

2.6.1 | Surgical Procedure

For the surgical procedures, the animals were initially weighed and then anesthetized with an intraperitoneal injection of a solution of Xylazine (20 mg/kg; Syntec, Tamboré, SP, Brazil) and Ketamine (80 mg/kg; Syntec, Tamboré, SP, Brazil). The surgical sites on the dorsal skin were shaved, and antisepsis of the area was performed using 2% chlorhexidine. The experimental cements (C_3S, CZS, SPS) and Biodentine (BD) were prepared and inserted into pre-sterilized polyethylene tubes. A total of 360 polyethylene tubes with an internal diameter of 1.0 mm, an external diameter of 1.6 mm, a length of 10.0 mm, and one open end were needed.

Subsequently, five equally spaced sections were marked, where 2-cm subcutaneous incisions were made using a #15 scalpel blade (Solidor, São Bernardo do Campo, SP, Brazil). Using blunt surgical scissors (Aesculap, Tuttlingen, Germany), pockets were created by gently separating the tissues to accommodate the tubes.

Each animal received five implants: one for each cement and one empty tube as control (CON). The end of the tube with the tested materials was inserted facing the bottom of the pockets, ensuring that the incision was opposite the analyzed material. Once the polyethylene tubes were inserted, the edges of all incisions were closed with 4.0 silk sutures (EthiconTM, Cincinnati, OH, USA). The animals were monitored until they recovered from anesthesia, and their behavior was observed daily to prevent any incidents that could compromise the experiment.

After the experimental periods, the animals were anesthetized again and shaved in the dorsal region. They were then sacrificed with an overdose of anesthetic. Initially, the implanted tubes were located by palpation; afterward, the area was dissected to include sufficient surrounding normal tissue. The tissues containing the tubes were collected and fixed in 10% buffered formalin in individual containers labeled with the animal's identification, group, and experimental period. The specimens were stored for 48 h.

2.6.2 | Laboratory Processing

After the 48 h fixation period, histotechnical processing for staining using the hematoxylin–eosin (HE) technique was performed as described [8].

For scanning the slides, the Pannoramic Desk equipment (3DHISTECH Ltd., Budapest, Hungary) was used. The images were saved for viewing with the CaseViewer application (3DHISTECH Ltd), which was used to capture 5 microfields from each slide at a magnification of 400×, allowing for subsequent cell counting using the ImageJ program. The histopathological events evaluated included: inflammatory infiltrate (polymorphonuclear and mononuclear cells), cellularity (fibroblasts), and vascularization (blood vessels).

2.7 | Statistical Analysis

All data, regardless of the type of test, were tabulated and analyzed using BioEstat 5.3 software (BioEstat, Belém, PA, Brazil). After checking for normality using the Shapiro–Wilk test, parametric data were analyzed using ANOVA, followed by the Tukey test (for radiopacity, dimensional stability, and compressive strength). Non-parametric data were analyzed using the Kruskal-Wallis test, followed by Dunn's post-test (for setting time, solubility, pH, calcium/strontium release, and biocompatibility). In all analyses, significance was set at 5%.

3 | Results

3.1 | Characterization of the Synthesized Cements

3.1.1 | Fourier Transform Infrared Spectroscopy

Figure 1 shows the infrared spectra of the synthesized silicate samples, C_3S (1a), CZS (1b), and SPS (1c), along with their main characteristic band assignments for the chemical bonds present in the samples.

For C_3S (Figure 1a), the vibrational stretching bands at approximately 950 cm^{-1} were attributed to Si-O bonds, while those at 450 cm^{-1} relate to angular deformations of O—Si—O bonds. The presence of bonds related to carbonate ions (CO_3^{2-}) is observed. The discrete band at 1650 cm^{-1} corresponds to O—H bonds from water molecules. The intense band at 3645 cm^{-1} also observed may be associated with the hydroxyl group from water absorbed on the surface of the material. The discrete band near 418 cm^{-1} corresponds to O—Ca—O bonds from bending vibrational modes without bridging.

Regarding the CZS sample (Figure 1b), the band observed at approximately 3400 cm^{-1} indicates the presence of O—H groups. In the wave number range of 860–1052 cm^{-1}, isolated SiO_4 groups were seen at 974, 950, 921, and 863 cm^{-1}. Bands in the wave number range of 600–800 cm^{-1} were attributed to Si—O—Si and Si—O, as well as lower wave numbers between 400 and 600 cm^{-1} for Si—O—Si bonds. Finally, the band at 408 cm^{-1} can also be attributed to the vibration of the O—Zr—O bond.

The FTIR spectrum of the SPS powder (Figure 1c) exhibited characteristic absorption bands indicating the presence of phosphate groups (PO_4^{3-}), as evidenced by vibrational bands at 567, 598, 1024, and 1076 cm^{-1}. The intense band appeared at 824 cm^{-1} due to the presence of silicate (SiO_4^{4-}). The broad and discrete vibrational bands at 3526 and 1635 cm^{-1} denote the stretching and bending modes of the O-H group related to moisture in the sample. Lastly, bands were described at wave numbers 505

and 824–917 cm^{-1} due to bending and stretching modes of Si-O bonds in SiO_4^{4-}.

3.1.2 | X-Ray Diffraction

Figure 2 displays the XRD patterns of the samples C_3S (2a), CZS (2b), and SPS (2c), respectively. Characteristic peaks of two crystalline phases were identified for the C_3S sample (Figure 2a), namely dicalcium silicate (Ca_2SiO_4), with peaks marked by the letter "d," and tricalcium silicate (Ca_3SiO_5), with peaks marked by the letter "t," along with their respective crystallographic data from the ICSD.

As observed in Figure 2b, the peaks described in the diffraction spectrum were compared with the pattern of the CZS sample found in the ICSD, allowing for the identification of most corresponding peaks of the pure phase of the structure $Ca_3ZrSi_2O_9$. Peaks related to the CZS phase corresponding to the planes (0 2 3) at 32.19°, (0 3 1) at 28.41°, and (1 0 0) at 14.95° were detected.

The diffraction patterns of SPS (Figure 2c) were mostly in agreement with the ICSD pattern, which may indicate the presence of a single phase for the structure $Sr_5(PO_4)_2SiO_4$.

3.1.3 | Scanning Electron Microscopy/Energy Dispersive Spectroscopy

Micrographs of the synthesized silicate samples with elemental mapping by EDS are presented in Figure 3: C_3S (a, b), CZS (c, d), and SPS (e, f).

As observed in Figure 3a, the morphology of the cement showed a granular shape with an amorphous characteristic, highlighting the presence of calcium in a higher molar proportion (Figure 3b). There is also a regularity in the diameter of the grains, with an average of 1.26 μm. The presence of the chemical elements calcium (Ca), silicon (Si), and oxygen (O) was evident in the micrographs, along with their mass proportions.

Regarding CZS, as seen in Figure 3c, the morphology shows a granular structure with homogeneous and well-defined dispersion, with an average grain diameter of 2.64 μm. The chemical elements present in the CZS sample (O, Zr, Si, and Ca) were identified and highlighted in color (Figure 3c), along with the mass proportions through the EDS spectrum (Figure 3d). The morphology of SPS is shown in Figure 3e,

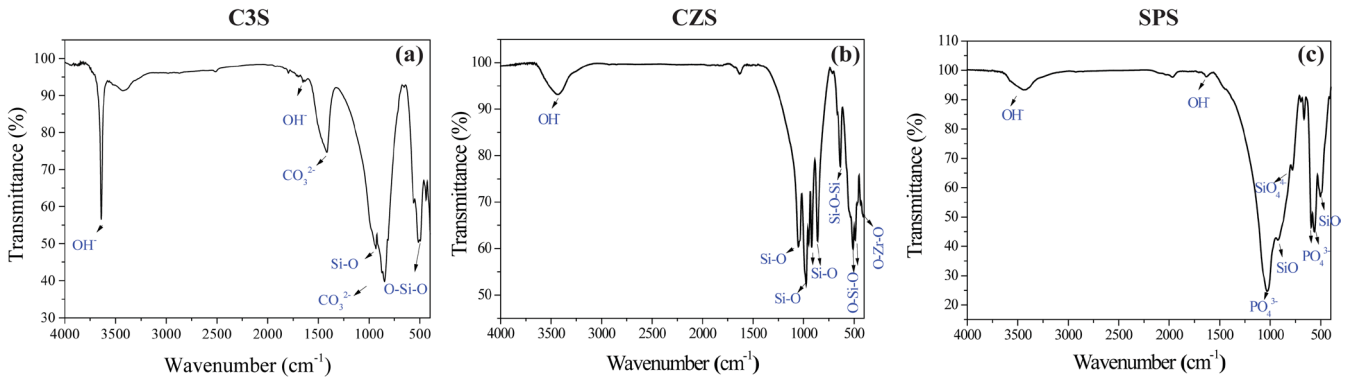

FIGURE 1 | FTIR spectra of C3S (a), CZS (b), and SPS (c) samples.

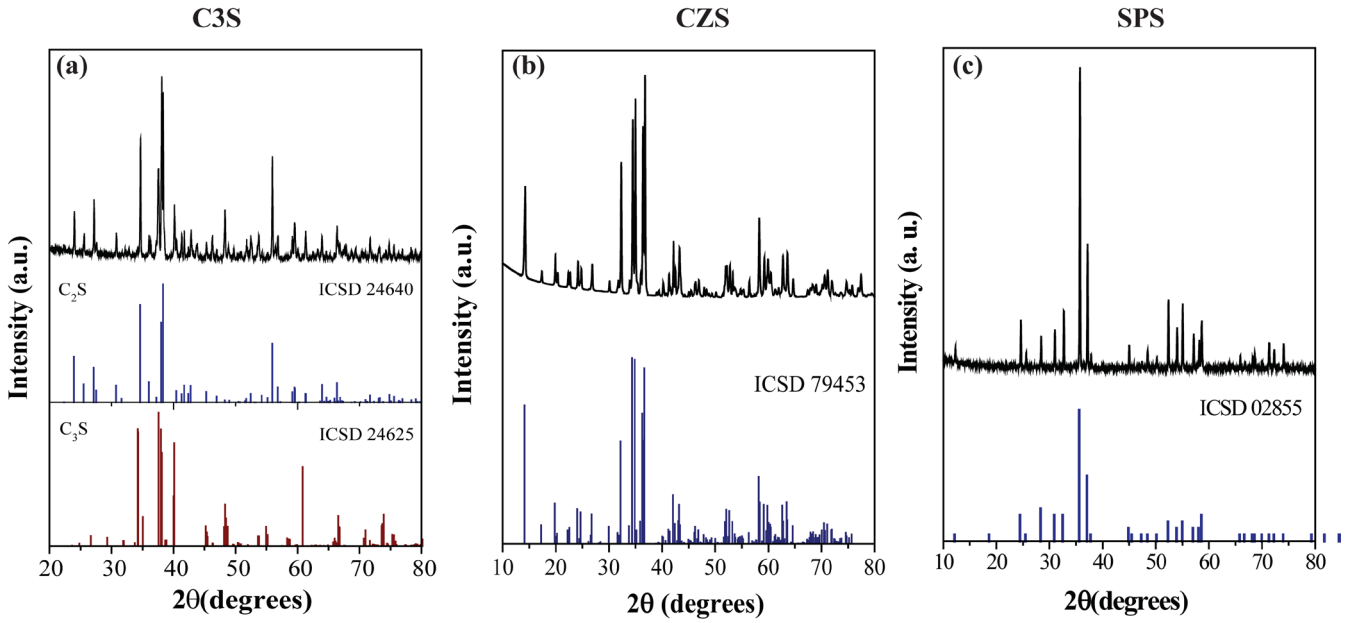

FIGURE 2 | XRD pattern of the powder after sintering at 1400°C of C3S (a), CZS (b), and SPS (c) samples.

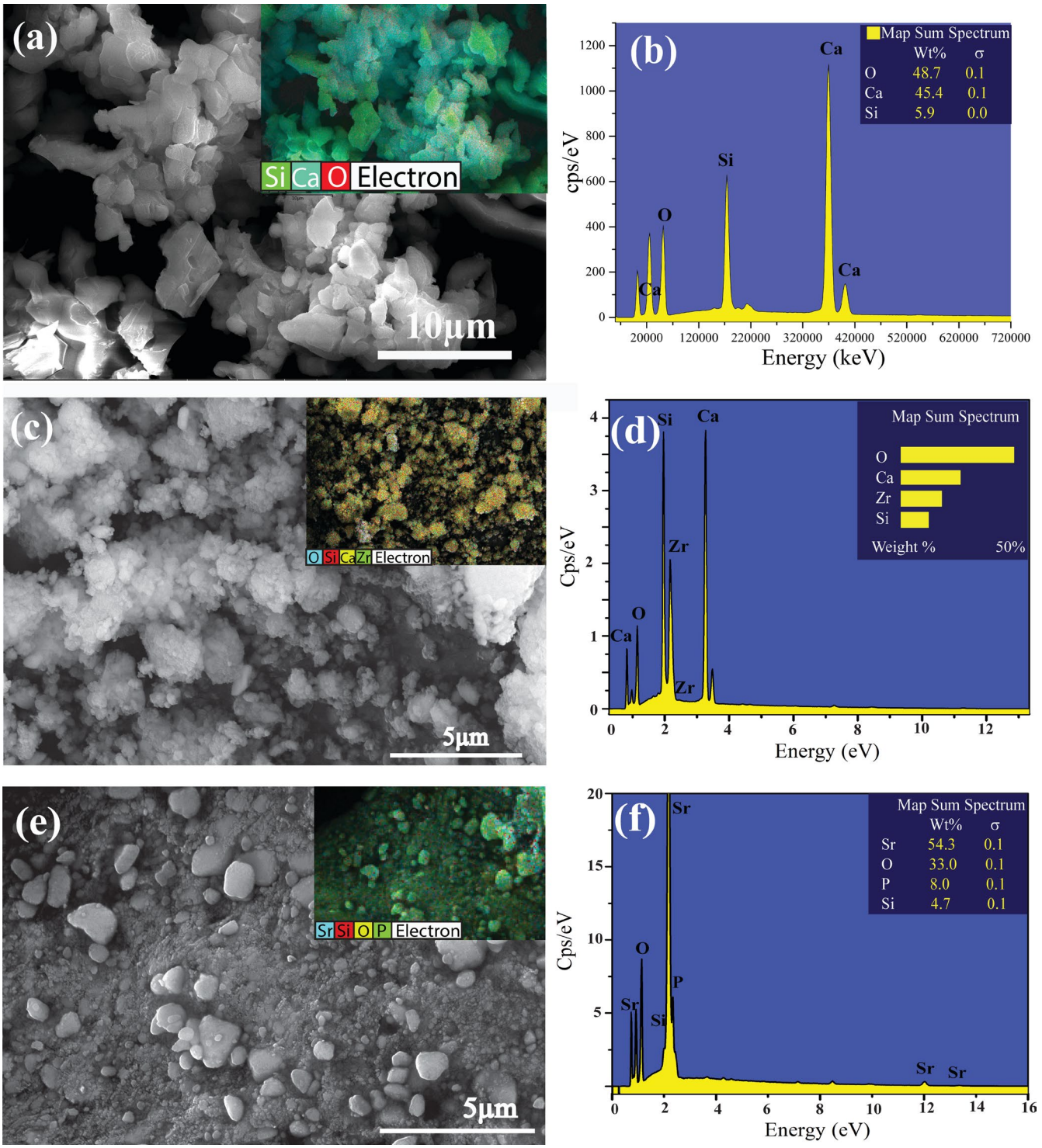

FIGURE 3 | SEM micrographs and EDS maps and elemental spectra of C3S (a, b), CZS (c, d), and SPS (e, f).

where a granular shape with a more oval aspect is evident compared to the other silicates. This sample exhibited a more defined morphology with oval grains of varying dimensions, averaging 1.50 µm. All the chemical elements of the SPS structure ($Sr_5(PO_4)_2SiO_4$) were identified (highlighted in color). Additionally, Figure 3f displays the EDS spectrum that identified the mass proportions of the constituent elements of the SPS sample.

3.1.4 | Transmission Electron Microscopy

Figure 4 presents images obtained from TEM of the samples C_3S (a–c), CZS (d–f), and SPS (g–i), respectively. The images in Figure 4a–c highlight the characteristics of the crystallites in the synthesized C_3S sample. Small clusters of crystallites were observed, with an average size of 12 nm, exhibiting a uniform and defined shape. In Figure 4c, the structure of some C_3S

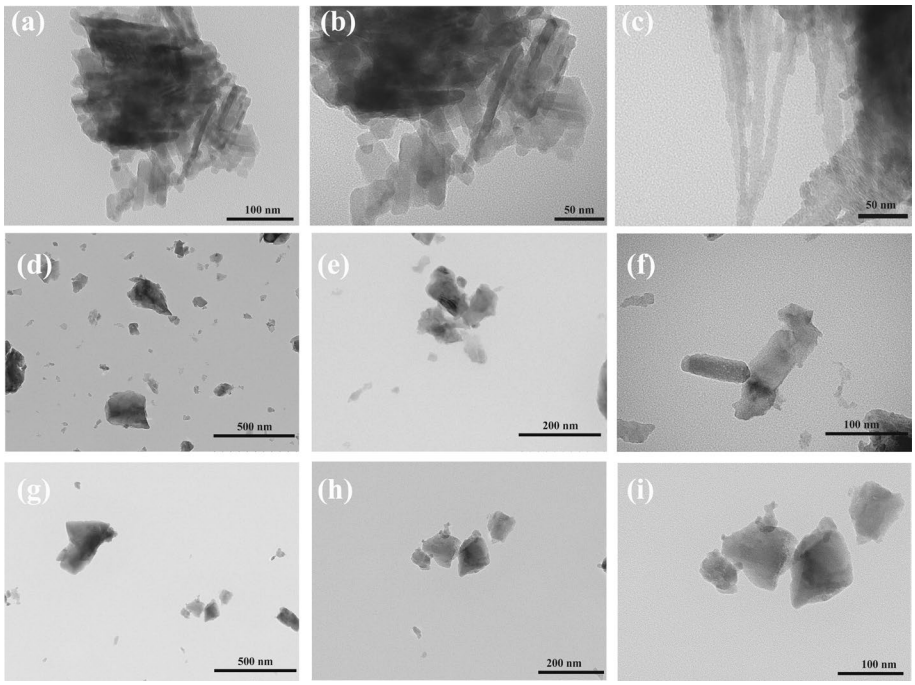

FIGURE 4 | TEM images of the sample (a–c) C3S, (d–f) CZS and (g–i) SPS.

nanoparticles is visible, showing a capillary form with notable clustering, which can also be described as elongated rods.

For the CZS sample, shown in Figure 4d–f, amorphous particles with little definition were observed. The average size of these particles was 55 nm, which is larger than the C_3S sample. Meanwhile, Figure 4g–i presents the micrographs of the SPS sample, which exhibited particles with irregular morphology and an average size of 46 nm.

3.2 | Physicochemical Properties

Table 1 presents the results of evaluations for physicochemical properties, including setting time, radiopacity, dimensional stability, compressive strength, and solubility. The cements exhibited the same order of results for both initial and final setting times: BD<SPS < CZS < C_3S. Significant differences were observed between BD and C_3S/CZS, as well as SPS and C_3S ($p < 0.05$).

In the radiopacity analysis, observations were made for the silicates with and without ZrO_2. The results revealed significant differences in comparisons between groups and within groups ($p < 0.05$). When including the radiopacifier, the materials ranked as SPS>CZS > C_3S > BD ($p < 0.05$). Without the radiopacifier, the order was SPS>CZS > C_3S ($p < 0.05$). Only the result for C_3S without the radiopacifier fell below 3 mm of aluminum (2.66 mm Al), as required by ISO 6876/2012 [18]. In the within-group analysis, the three EHCs with added radiopacifier showed significant differences compared to those without ($p < 0.05$).

In the dimensional stability analysis (%) at 24 h and 30 days, no significant differences were identified between the groups ($p > 0.05$), nor in comparisons between periods for the same material ($p > 0.05$). Regarding compressive strength (MPa), significant differences were observed between BD and the other cements ($p < 0.05$) at both 24 h and 30 days. Additionally, at 30 days, significant differences were noted between CZS and SPS ($p < 0.05$). In comparing compressive strength between periods for the same cement, significant differences were found in all EHCs ($p < 0.05$), resulting from increased values after 30 days of storage.

In the solubility analysis (%) at 24 h, a significant difference was noted between BD and the other cements, with BD exhibiting the lowest mass loss ($p < 0.05$). Additionally, there was a significant difference between C_3S and CZS/SPS ($p < 0.05$). At 30 days, significant differences were found between BD and the cements C_3S/SPS ($p < 0.05$). All cements, except for BD, did not comply with ANSI/ADA #57 [23], exhibiting solubility above 3%.

Table 2 presents the pH values found for each material across different periods. Significant differences were noted between BD and C_3S/CZS at 3 h and 15 days ($p < 0.05$), with BD samples associated with the highest pH. No differences were noted between groups at 24 h and 30 days ($p > 0.05$). At 72 h, significant differences were observed between C_3S and SPS/BD ($p < 0.05$), with C_3S showing the highest pH. At 168 h, significant differences were observed between C_3S and CZS/BD ($p < 0.05$), with C_3S samples again associated with the highest pH.

Regarding the analysis of calcium/strontium ion release capacity (mg/dL), the presence of these ions was not detectable in the controls. The values obtained for the cements are available in Table 3. At 3 h, a significant difference was observed between SPS and the other cements ($p < 0.05$), with SPS samples associated with lower ionic release. At 24, 72, 168, 15 days, and 30 days, significant differences were noted for the SPS group compared to C_3S and CZS ($p < 0.05$), with SPS samples exhibiting higher

TABLE 1 | Central tendency measures presented by the cements for the properties of setting time, radiopacity, dimensional stability, compressive strength, and solubility.

			C_3S		CZS		SPS		BD	
Tests			**Median**	**(min.–max.)**	**Median**	**(min.–max.)**	**Median**	**(min.–max.)**	**Median**	**(min.–max.)**
Setting time (min)	Initial		56^{c}	(53–59)	31^{bc}	(31–33)	21^{ab}	(19–24)	11^{a}	(10–13)
	Final		106^{c}	(105–127)	68^{bc}	(68–70)	50^{ab}	(48–51)	16^{a}	(15–20)
			Mean	**SD**	**Mean**	**SD**	**Mean**	**SD**	**Mean**	**SD**
Radiopacity (mm Al)		With radiopac.	9.41^{cA}	0.78	13.96^{bA}	1.09	19.03^{aA}	1.14	3.39^{d}	0.21
		Without radiopac.	2.66^{cB}	0.44	7.71^{bB}	0.36	12.81^{aB}	0.6	—	—
			Mean	**SD**	**Mean**	**SD**	**Mean**	**SD**	**Mean**	**SD**
Dimensional stability (%)		24 h	$0.26^{a,A}$	0.5	$0.62^{a,A}$	0.63	$0.44^{a,A}$	0.27	$0.99^{a,A}$	0.91
		30 days	$0.44^{a,A}$	0.51	$0.13^{a,A}$	0.22	$0.65^{a,A}$	0.48	$0.65^{a,A}$	0.77
			Mean	**SD**	**Mean**	**SD**	**Mean**	**SD**	**Mean**	**SD**
Compressive strength (MPa)		24 h	$2.65^{b,B}$	0.66	$2.79^{b,B}$	0.42	$1.59^{b,B}$	0.27	$141.53^{a,A}$	10.43
		30 days	$15.47^{bc,A}$	2.21	$17.20^{b,A}$	2.58	$4.36^{c,A}$	0.58	$91.81^{a,B}$	16.28
			Median	**(min.–max.)**	**Median**	**(min.–max.)**	**Median**	**(min.–max.)**	**Median**	**(min.–max.)**
Solubility (%)	24 h		2.45^{b}	(2.20–2.70)	3.17^{c}	(3.08–3.39)	3.86^{c}	(3.57–4.36)	0.40^{a}	(0.35–0.57)
	30 days		3.91^{b}	(3.49–4.27)	3.30^{ab}	(2.96–3.60)	3.78^{b}	(3.37–4.00)	2.41^{a}	(1.25–2.86)

Note: Lowercase letters (a, b) that are different and superscripted indicate significant differences between experimental groups. Uppercase letters that are different and superscripted indicate significant differences within groups; parametric analyses employed ANOVA and Tukey tests, while non-parametric analyses used Kruskal-Wallis and Dunn tests, with $p < 0.05$.

values, indicating an inversion from the 3 h results. In these periods, no differences were found between the SPS and BD cements ($p > 0.05$).

3.3 | Biocompatibility Testing

Figure 5 presents the graph, while Figures 6 (10×), 7, 8 and 9 (40×) show illustrative histological sections from the biocompatibility analysis of the control (CON), BD, C_3S, CZS, and SPS samples at 15, 30, and 60 days. Overall, the HE-stained sections revealed that the inflammatory reaction induced by the materials was localized in the connective tissue, closely adjacent to the openings of the polyethylene tubes. No inflammatory infiltrate was observed in the surrounding loose connective and muscle tissues.

Polymorphonuclear cells, mononuclear cells, and fibroblasts did not differ among the groups in each individual evaluation period ($p > 0.05$). However, for the occurrence of blood vessels, significant differences were noted at 30 days, with the BD, C_3S, and CZS groups exhibiting lower vascularization compared to the control (CON) and SPS groups ($p < 0.05$).

When considering different periods for the same material, differences in polymorphonuclear cell counts were observed between 60 days and the shorter evaluation periods across all groups ($p < 0.05$), indicating a reduced inflammatory infiltrate. The exception was the BD group at 30 days, which was similar to 60 days ($p > 0.05$); a significant difference was also noted in BD between 30 and 15 days ($p < 0.05$). For mononuclear cells and fibroblasts, differences were observed between the 30 and 60-day periods compared to the 15 days period for all groups evaluated ($p < 0.05$), with the 30- and 60-days periods associated with a lower quantity of mononuclear cells and fibroblasts.

4 | Discussion

The search for new materials is seen as natural because no product currently available meets the ideal characteristics for an endodontic repair cement. Starting from hydraulic repair cements based on calcium silicates, the present study aimed to synthesize and characterize three silicates, namely: tricalcium silicate, calcium zirconium silicate, and strontium phosphate silicate, and subsequently prepare EHCs from them, evaluating their physicochemical properties and biocompatibility. Overall, the results indicated that the EHCs performed consistently with their intended application, with some properties comparable to BD, the currently preferred repair material, while in other analyses, EHCs were inferior, leading to the rejection of the proposed statistical hypothesis.

Physicochemical analyses required the characterization of the synthesized substances [24]. FTIR results showed bands consistent with the expected composition of C_3S [25, 26], CZS [27],

TABLE 2 | Values (median and min.–max) of hydroxyl ion release obtained from the evaluated cements.

	C_3S		CZS		SPS		BD	
Periods	**Median**	**(min.–max.)**	**Median**	**(min.–max.)**	**Median**	**(min.–max.)**	**Median**	**(min.–max.)**
3 h	7.15^{b}	(6.74–9.05)	6.90^{b}	(6.57–8.75)	7.56^{ab}	(7.09–8.27)	8.70^{a}	(7.28–9.14)
24 h	8.28^{a}	(6.36–8.74)	7.98^{a}	(6.07–8.95)	8.60^{a}	(8.11–8.95)	8.57^{a}	(7.79–9.23)
72 h	9.50^{a}	(9.06–9.65)	8.83^{ab}	(8.74–10.23)	8.77^{b}	(7.47–9.28)	8.80^{b}	(7.14–9.16)
168 h	9.23^{a}	(7.22–9.49)	8.71^{b}	(6.73–8.89)	8.95^{ab}	(7.51–9.12)	8.59^{b}	(7.00–9.07)
15 days	7.31^{b}	(7.14–7.67)	7.37^{b}	(7.09–7.51)	7.67^{ab}	(7.14–7.86)	7.99^{a}	(7.43–8.84)
30 days	7.06^{a}	(6.91–7.20)	7.15^{a}	(6.85–7.68)	6.96^{a}	(6.09–7.33)	7.06^{a}	(6.63–8.79)

Note: Different superscript letters (a, b) indicate significant differences between experimental groups in the evaluated periods according to the Kruskal-Wallis and Dunn tests, with $p < 0.05$.

TABLE 3 | Values (median and min.-max) of calcium/strontium ion release (mg/dL) obtained from the evaluated cements.

	C_3S		CZS		SPS		BD	
Periods	**Median**	**(min.–max.)**	**Median**	**(min.–max.)**	**Median**	**(min.–max.)**	**Median**	**(min.–max.)**
3 h	24.59^{a}	(19.15–29.50)	14.35^{a}	(5.46–31.83)	6.02^{b}	(4.79–7.26)	14.29^{a}	(9.31–23.25)
24 h	5.12^{bc}	(2.99–6.94)	1.95^{c}	(1.62–2.82)	8.31^{a}	(7.36–9.09)	5.37^{ab}	(3.78–6.32)
72 h	1.91^{bc}	(1.17–9.90)	1.82^{c}	(0.55–2.71)	10.94^{a}	(9.80–13.03)	5.50^{ab}	(4.58–7.44)
168 h	1.27^{c}	(0.83–3.37)	2.46^{bc}	(1.93–3.38)	12.62^{a}	(9.71–16.95)	6.73^{ab}	(5.22–10.28)
15 days	2.66^{c}	(1.61–7.15)	3.38^{bc}	(2.60–4.43)	11.27^{a}	(8.92–15.87)	6.73^{ab}	(5.22–10.28)
30 days	2.99^{b}	(2.02–3.82)	4.78^{b}	(3.70–5.81)	12.03^{a}	(5.91–20.22)	12.74^{a}	(7.63–16.13)

Note: Different superscript letters (a, b) indicate significant differences between experimental groups in the evaluated periods according to the Kruskal-Wallis and Dunn tests, with $p < 0.05$.

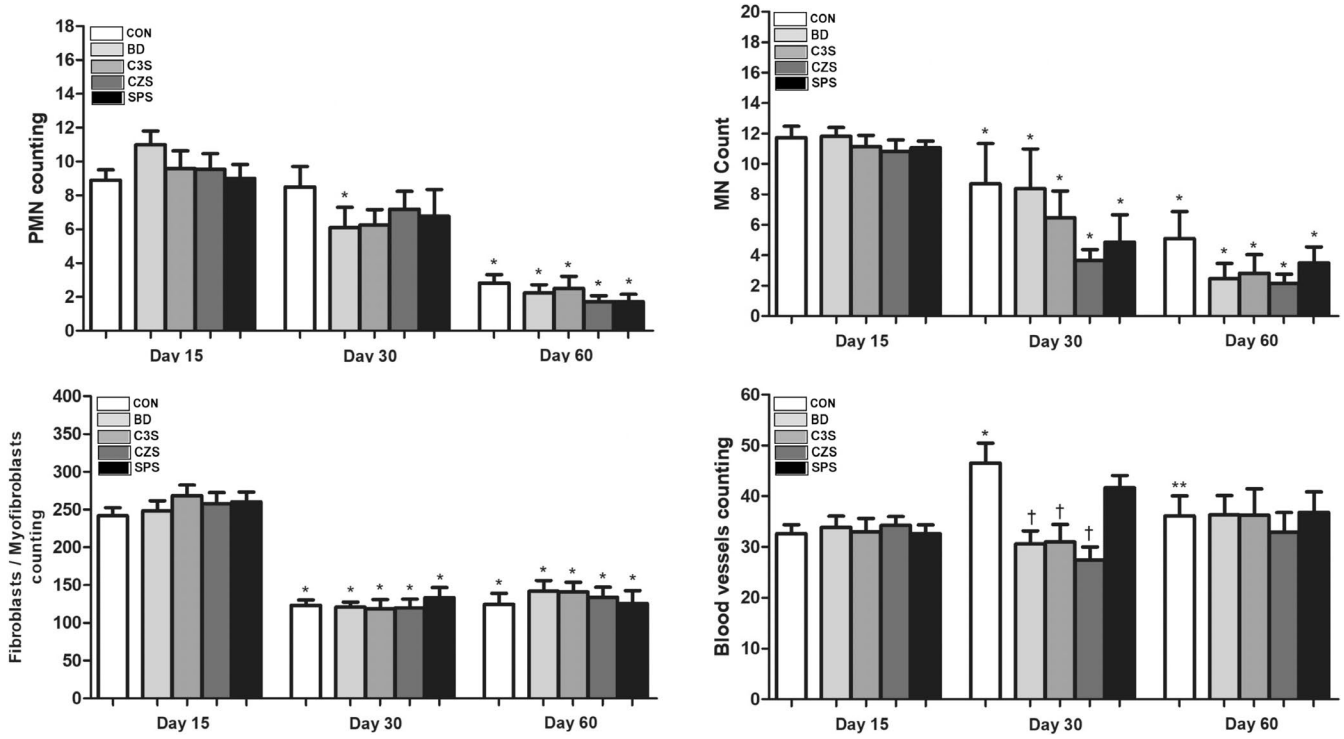

FIGURE 5 | Graphical representation of the biocompatibility of the evaluated cements: BD, biodentine; C3S, tricalcium silicate; CON, control; CZS, calcium zirconium silicate, SPS, strontium phosphate silicate. Different capital letters represent significant differences between groups on the same day. Different symbols (*$p < 0.05$ vs. D15; **$p < 0.05$ vs. D30; †$p < 0.05$ vs. C) represent significant differences between days in the same group according to the Kruskal-Wallis/Dunn test (mean ± SEM) ($p < 0.05$).

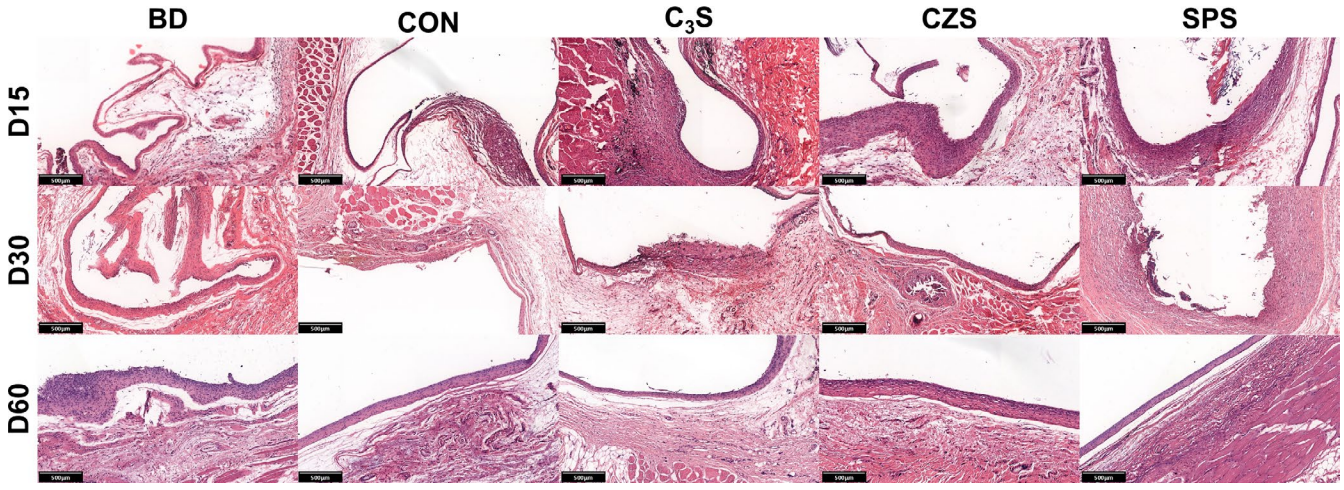

FIGURE 6 | Representation of photomicrographs of the histopathological analysis (H&E) of the subcutaneous pocket, at lower magnification (10×), the site of inoculation of the filling materials (central blank area) after removal of the retaining tubes. The tissue is surrounded by an inflammatory infiltrate, which is intense 15 days after the surgical procedure and gradually replaced by a thin capsule of granulation tissue after 30 days and by fibrosis from 60 days onward. No signs of toxicity were observed.

and SPS [28]. XRD analysis revealed that C_3S formed two crystalline phases: dicalcium silicate (Ca_2SiO_4) and tricalcium silicate (Ca_3SiO_5), with peaks matching standard C_3S references [29]. CZS and SPS samples also showed excellent agreement with their characteristic crystalline phases, demonstrating successful synthesis according to the proposed methods (ICSD).

The synthesis methods were selected to produce nanoparticles while minimizing undesirable crystalline phases. All samples contained predominantly small grains, which can reduce interparticle spaces, improving cohesion and providing a larger contact area with the environment. This may enhance adaptation, sealing, and resistance to displacement [7]. EDS analysis confirmed the absence of contaminants such as Al or Fe; aluminum

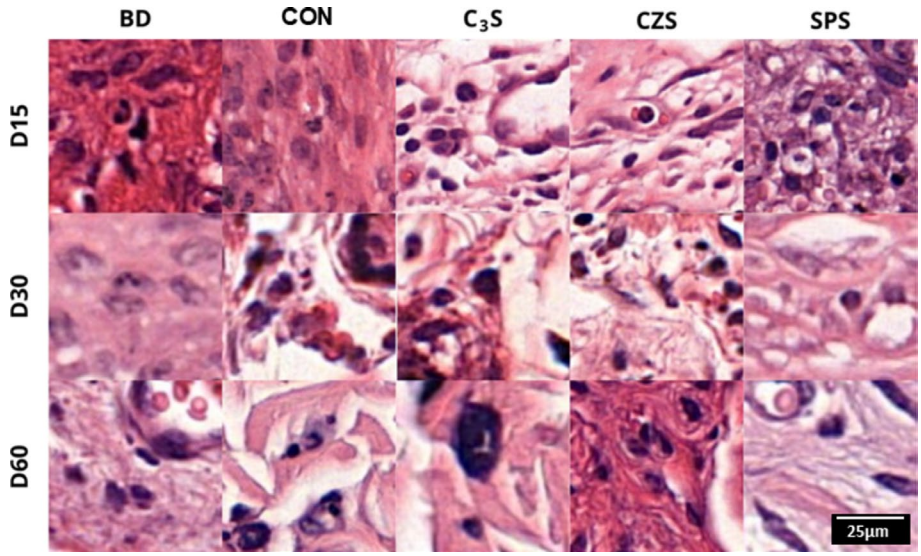

FIGURE 7 | Representation of photomicrographs of the histopathological analysis (H&E) of the subcutaneous pocket showing neutrophils in the three experimental periods (15, 30, and 60 days) of the BD, C, C3S, CZS and SPS groups. All groups exhibited an intense infiltrate during the first 15 days following the inoculation of the materials into the dorsal region of the animals. After 30 days, all endodontic cements showed a significant reduction in the number of PMN cells, and only the control group still displayed a persistent inflammatory infiltrate at this time point. From day 60 onward, the connective tissue showed almost no PMN cells, being composed mainly of mononuclear cells and fibrocytes.

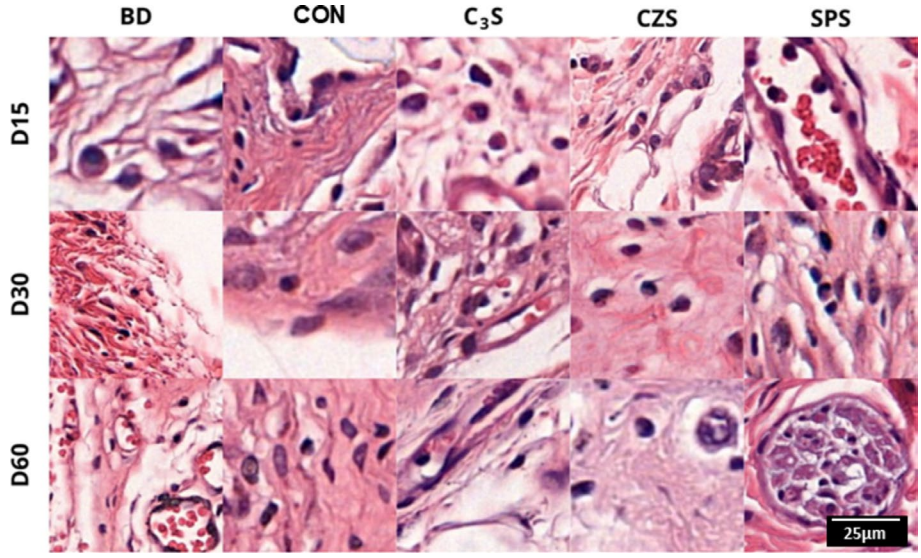

FIGURE 8 | Representation of photomicrographs of the histopathological analysis (H&E) of the subcutaneous pocket showing monocytes in the three experimental periods (15, 30, and 60 days) of the BD, C, C3S, CZS and SPS groups. Predominantly composed of macrophages and occasional plasma cells, the MN infiltrate showed a significant reduction in all groups between days 15 and 30 after cement inoculation into the dorsal region of the animals, maintaining this pattern up to Day 60.

is linked to Alzheimer's disease [30], while iron can alter material color.

Regarding setting times, the materials exhibited a similar ordering, indicating consistent hardening behavior. BD had the shortest setting times, consistent with literature [31, 32], similar to SPS, while C_3S and CZS exhibited longer times comparable to other MTA-based cements [33, 34]. Regardless of this aspect, it is important to highlight that different proportions of propylene/water and even powder/liquid could result in shorter setting times.

Regarding the radiopacity results, the values found for SPS were remarkable; this characteristic of Sr. draws attention to the sum of a functional bone deposition interaction and a radiopacifying action inherent to its molecular weight. C_3S did not initially meet radiopacity standards, but the addition of ZrO_2 enabled compliance. BD's radiopacity results were consistent with literature, highlighting its relatively low radiopacity [9, 31, 35, 36]. These findings suggest the possibility of carrying out new studies even without the inclusion of a radiopacifier in cements prepared with either SPS or CZS, which could alter some of the results found here.

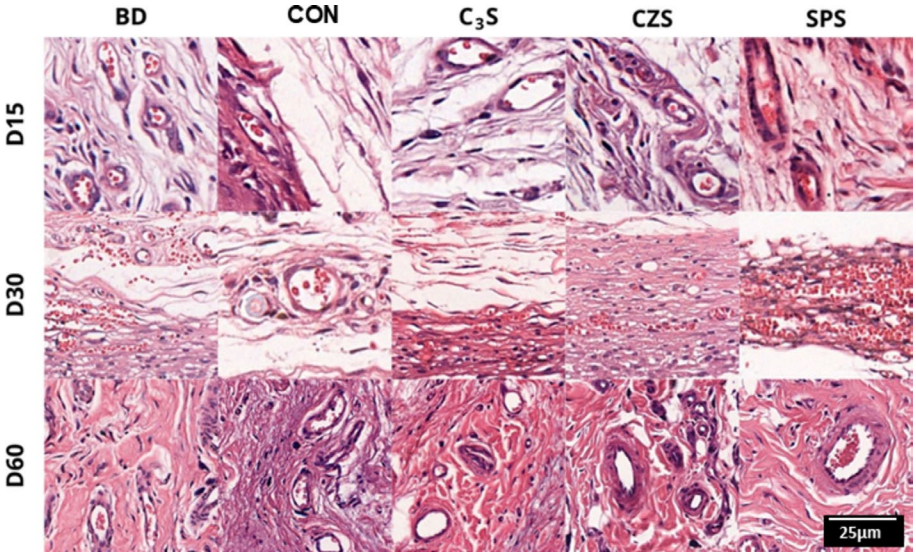

FIGURE 9 | Representation of photomicrographs of the histopathological analysis (H&E) of the subcutaneous pocket showing fibroblasts and vessels in the three experimental periods (15, 30 and 60 days) of the BD, C, C3S, CZS and SPS groups. Vascular neoformation and collagen deposition following the inoculation of the cements into the dorsal region of the animals could be seen. On day 15, numerous fibroblasts and myofibroblasts were observed in all experimental groups, associated with occasional collagen fibers. At 30 and 60 days after material inoculation, the number of fibroblasts significantly decreased, accompanied by an increase in the density of deposited collagen fibers. Specifically, in the control and SPS groups, an increase in the number of blood vessels was observed after day 30, with vessels appearing interspersed among newly deposited collagen fibers. In the remaining groups, the increase in vascularization occurred only after 60 days, when the distribution within the connective tissue became similar among all experimental groups.

Dimensional stability was similar among EHCs and BD, with all cements meeting ISO 6876/2012 and ANSI/ADA 2000 standards [18, 23], in line with previous reports [37, 38]. Compressive strength was higher in BD due to its low water/cement ratio and polymer content [9]; EHCs, although lower, performed comparably to other MTA-based cements [39]. Solubility was lowest in BD, likely due to its low water content [40], whereas EHCs slightly exceeded standard limits but were similar to other MTA-based cements [39, 41]. Given the bio-stimulating effects of environmental alkalinization and calcium ion release [31, 42], this solubility may be advantageous.

Alkalinity is crucial for repair, but excessive levels can cause chemical injury [42]. All materials exhibited appropriate alkalinizing potential, consistent with recent literature [35, 43–45], generally increasing up to 72/168 h, with C3S showing the most pronounced effect. After 15 days, alkalinity decreased gradually, and by 30 days, values were similar among all cements, consistent with other hydraulic cements [35, 44, 45]. C3S released calcium ions more rapidly initially than SPS, but release diminished over time, likely reflecting initial hydration influenced by the powder/liquid ratio [39]. Ion release was comparable to BD, known for high calcium ion availability due to its composition and rapid hydration [39, 46].

Biocompatibility is indicated by minimal inflammatory response over time [47]. All groups showed moderate initial inflammation, which later subsided to mild levels, without statistical differences from controls, confirming biocompatibility [8, 42, 48–50]. Despite compositional differences, EHCs and BD elicited similar tissue responses, likely due to shared silica particles and the release of calcium/strontium and hydroxide ions [50, 51]. Fibroblast recruitment relative to inflammatory cells indicated active tissue repair, with thin collagen capsule formation observed after final setting [52]. SPS also promoted significantly higher neovascularization at 30 days, potentially due to Sr. stimulating proangiogenic factors [24].

In light of the many data collected in this study and the potential for developing new biomaterials to be used as repair cements in cases of perforation, apical sealing, and revascularization procedures in cases of incomplete rhizogenesis, the findings reported here suggest that the proposed EHCs exhibit physical–chemical properties and biocompatibility compatible with their intended use, demonstrating promise for clinical applications, pending further in vivo studies. However, it should be emphasized that the results of laboratory studies cannot be directly extrapolated to clinical conditions. Nonetheless, considering this study as an initial step in the development of these EHCs, the comparison with BD undeniably shows that further studies are needed to enhance certain characteristics, actively working on their composition to include auxiliary substances that could improve some of their properties. Such modifications could yield cements with different physical–chemical characteristics, which should be the subject of future studies.

5 | Conclusion

Based on the above and considering the conditions of the present study, it can be concluded that the proposed EHCs were synthesized in a pure phase and exhibited promising physicochemical properties and adequate biocompatibility.

Acknowledgments

The TEM analyses were conducted in collaboration with the Center for the Development of Nanoscience and Nanotechnology (CEDENNA),

Chile. The biocompatibility analyses were carried out in partnership with the Experimental Biology Center (NUBEX) at the University of Fortaleza, Brazil. This study was partially funded by Coordination for the Improvement of Higher Education Personnel of the Ministry of Education of Brazil and FUNCAP—Ceará Foundation to Support Scientific and Technological Development. The authors declare no competing interests. The Article Processing Charge for the publication of this research was funded by the Coordenação de Aperfeiçoamento de Pessoal de Nível Superior - Brasil (CAPES) (ROR identifier: 00x0ma614).

Funding

This work was supported by Coordenação de Aperfeiçoamento de Pessoal de Nível Superior and Fundação Cearense de Apoio ao Desenvolvimento Científico e Tecnológico (UNI-210-00671.01.00/23).

Conflicts of Interest

The authors declare no conflicts of interest.

Data Availability Statement

The data that support the findings of this study are available from the corresponding author upon reasonable request.

References

1. F. Eskandari, A. Razavian, R. Hamidi, K. Yousefi, and S. Borzou, "An Updated Review on Properties and Indications of Calcium Silicate-Based Cements in Endodontic Therapy," *International Journal of Dentistry* 2022 (2022): 6858088.

2. A. Eshghi, M. Hajiahmadi, M. H. Nikbakht, and M. Esmaeili, "Comparison of Clinical and Radiographic Success Between MTA and Biodentine in Pulpotomy of Primary Mandibular Second Molars With Irreversible Pulpitis: A Randomized Double-Blind Clinical Trial," *International Journal of Dentistry* 2022 (2022): 6963944.

3. R. A. B. Silva, P. Gaton-Hernandez, C. M. Pucinelli, et al., "Subcutaneous Tissue Reaction and Gene Expression of Inflammatory Markers After Biodentine and MTA Implantation," *Brazilian Dental Journal* 33 (2022): 41–56.

4. J. Camilleri, "Color Stability of White Mineral Trioxide Aggregate in Contact With Hypochlorite Solution," *Journal of Endodontics* 40 (2014): 436–440.

5. A. Nowicka, M. Lipski, M. Parafiniuk, et al., "Response of Human Dental Pulp Capped With Biodentine and Mineral Trioxide Aggregate," *Journal of Endodontics* 39 (2013): 743–747.

6. L. Awawdeh, A. Al-Qudah, H. Hamouri, and R. J. Chakra, "Outcomes of Vital Pulp Therapy Using Mineral Trioxide Aggregate or Biodentine: A Prospective Randomized Clinical Trial," *Journal of Endodontics* 44 (2018): 1603–1609.

7. B. A. Aguiar, L. M. A. Frota, D. T. Taguatinga, et al., "Influence of Ultrasonic Agitation on Bond Strength, Marginal Adaptation, and Tooth Discoloration Provided by Three Coronary Barrier Endodontic Materials," *Clinical Oral Investigations* 23 (2019): 4113–4122.

8. T. A. Souza, M. M. Bezerra, P. G. B. Silva, et al., "Bone Morphogenetic Proteins in Biomineralization of Two Endodontic Restorative Cements," *Journal of Biomedical Materials Research. Part B, Applied Biomaterials* 109 (2021): 348–357.

9. J. Camilleri, F. Sorrentino, and D. Damidot, "Investigation of the Hydration and Bioactivity of Radiopacified Tricalcium Silicate Cement, Biodentine and MTA Angelus," *Dental Materials* 29 (2013): 580–593.

10. M. A. H. Duarte, M. A. Marciano, R. R. Vivan, M. Tanomaru Filho, J. M. G. Tanomaru, and J. Camilleri, "Tricalcium Silicate-Based Cements: Properties and Modifications," *Brazilian Oral Research* 32 (2018): e70.

11. N. Z. Arandi and M. Thabet, "Minimal Intervention in Dentistry: A Literature Review on Biodentine as a Bioactive Pulp Capping Material," *BioMed Research International* 2021 (2021): 5569313.

12. E. Bonnelye, A. Chabadel, F. Saltel, and P. Jurdic, "Dual Effect of Strontium Ranelate: Stimulation of Osteoblast Differentiation and Inhibition of Osteoclast Formation and Resorption in Vitro," *Bone* 42 (2008): 129–138.

13. T. Wu, S. Yang, T. Lu, et al., "Strontium Ranelate Simultaneously Improves the Radiopacity and Osteogenesis of Calcium Phosphate Cement," *Biomedical Materials* 14 (2019): 35005.

14. U. Thormann, S. Ray, U. Sommer, et al., "Bone Formation Induced by Strontium Modified Calcium Phosphate Cement in Critical Size Metaphyseal Fracture Defects in Ovariectomized Rats," *Biomaterials* 34 (2013): 8589–8598.

15. M. Wu, T. Wang, Y. Wang, F. Li, M. Zhou, and X. Wu, "A Novel and Facile Route for Synthesis of Fine Tricalcium Silicate Powders," *Materials Letters* 227 (2018): 187–190.

16. T. C. Schumacher, A. Aminian, E. Volkmann, et al., "Synthesis and Mechanical Evaluation of Sr-Doped Calcium-Zirconium-Silicate (Baghdadite) and Its Impact on Osteoblast Cell Proliferation and ALP Activity," *Biomedical Materials* 10 (2015): 55013.

17. F. Deng, F. Wang, Z. Liu, H. Kou, G. Cheng, and C. Ning, "Enhanced Mechanical Property of $Ca_5(PO_4)_2SiO_4$ Bioceramic by a Biocompatible Sintering Aid of Zinc Oxide," *Ceramics International* 44 (2018): 18352–18362.

18. International Organization for Standardization, *ISO 6876: Dental Root Canal Sealing Materials*, ed. International Organization for Standardization (2012).

19. J. R. Carvalho-Junior, L. Correr-Sobrinho, A. B. Correr, M. A. Sinhoreti, S. Consani, and M. D. Sousa-Neto, "Solubility and Dimensional Change After Setting of Root Canal Sealers: A Proposal for Smaller Dimensions of Test Samples," *Journal of Endodontics* 33 (2007): 1110–1116.

20. A. Bernardi, E. A. Bortoluzzi, W. T. Felippe, M. C. Felippe, W. S. Wan, and C. S. Teixeira, "Effects of the Addition of Nanoparticulate Calcium Carbonate on Setting Time, Dimensional Change, Compressive Strength, Solubility and pH of MTA," *International Endodontic Journal* 50 (2017): 97–105.

21. G. C. Vertuan, M. A. H. Duarte, I. G. Moraes, et al., "Evaluation of Physicochemical Properties of a New Root Canal Sealer," *Journal of Endodontics* 44 (2018): 501–505.

22. H. M. Pessoa, R. A. Hauser-Davis, R. C. Campos, E. V. R. Castro, M. T. W. D. Carneiro, and G. P. Brandão, "Determination of Ca, Mg, Sr and Ba in Crude Oil Samples by Atomic Absorption Spectrometry," *Journal of Analytical Atomic Spectrometry* 27 (2012): 1568–1573.

23. American National Standards Institute/American Dental Association, *(ANSI/ADA) Specification No. 57: Endodontic Sealing Material*, ed. American National Standards/American Dental Association (2000).

24. H. Chang, H. Xiang, Z. Yao, et al., "Strontium-Substituted Calcium Sulfate Hemihydrate/Hydroxyapatite Scaffold Enhances Bone Regeneration by Recruiting Bone Mesenchymal Stromal Cells," *Journal of Biomaterials Applications* 35 (2020): 97–107.

25. M. M. Radwan, S. Nagi, and H. K. El-Hamid, "Physico-Mechanical Characteristics of Tri-Calcium Silicate Pastes as Dentin Substitute and Interface Analysis in Class II Cavities: Effect of $CaCl_2$ and SBF Solutions," *Heliyon* 5 (2019): e01975.

26. J. Higl, D. Hinder, C. Rathgeber, B. Ramming, and M. Lindén, "Detailed in Situ ATR-FTIR Spectroscopy Study of the Early Stages of CSH Formation During Hydration of Monoclinic C3S," *Cement and Concrete Research* 142 (2021): 106367.

27. S. Vaez, R. Emadi, S. Sadeghzade, H. Salimijazi, and M. Kharaziha, "Electrophoretic Deposition of Chitosan Reinforced Baghdadite Ceramic Nano-Particles on the Stainless Steel 316L Substrate to Improve

Biological and Physical Characteristics," *Materials Chemistry and Physics* 282 (2022): 125991.

28. A. Udduttula, J. Li, P. Y. Zhao, G. C. Wang, J. V. Zhang, and P. G. Ren, "Sol-Gel Derived Nanosized $Sr_5(PO_4)_2SiO_4$ Powder With Enhanced in Vitro Osteogenesis and Angiogenesis for Bone Regeneration Applications," *Ceramics International* 45 (2019): 3148–3358.

29. K. Mohan and F. P. Glasser, "The Thermal Decomposition of Ca_3SiO_5 at Temperatures Below 125o°: Part 3. The Influence of Water and Sulphate on the Decomposition," *Cement and Concrete Research* 7 (1977): 379–383.

30. W. F. Forbes and J. F. Gentleman, "Risk Factors, Causality, and Policy Initiatives: The Case of Aluminum and Mental Impairment," *Experimental Gerontology* 33 (1998): 141–154.

31. L. E. Pelepenko, F. Saavedra, T. B. M. Antunes, et al., "Physicochemical, Antimicrobial, and Biological Properties of White-MTAFlow," *Clinical Oral Investigations* 25 (2021): 663–672.

32. M. Domingos Pires, J. Cordeiro, I. Vasconcelos, et al., "Effect of Different Manipulations on the Physical, Chemical and Microstructural Characteristics of Biodentine," *Dental Materials* 37 (2021): 399–406.

33. C. P. Lucas, R. Viapiana, R. Bosso-Martelo, J. M. Guerreiro-Tanomaru, J. Camilleri, and M. Tanomaru-Filho, "Physicochemical Properties and Dentin Bond Strength of a Tricalcium Silicate-Based Retrograde Material," *Brazilian Dental Journal* 28 (2017): 51–56.

34. J. A. Duque, S. L. Fernandes, J. P. Bubola, M. A. H. Duarte, J. Camilleri, and M. A. Marciano, "The Effect of Mixing Method on Tricalcium Silicate-Based Cement," *International Endodontic Journal* 51 (2018): 69–78.

35. C. Z. Rabello, P. M. P. Kopper, L. J. M. Ferri, et al., "Physicochemical Properties of Three Bioceramic Cements," *Brazilian Oral Research* 36 (2022): 069.

36. L. B. Campi, F. F. E. Torres, E. M. Rodrigues, J. M. Guerreiro-Tanomaru, and M. Tanomaru-Filho, "Physicochemical and Biological Properties of New Tricalcium Silicate-Based Repair Material Doped With Fluoride Ions and Zirconium Oxide as Radiopacifier," *Journal of Biomedical Materials Research. Part B: Applied Biomaterials* 110 (2022): 862–870.

37. F. F. E. Torres, R. Bosso-Martelo, C. G. Espir, J. A. Cirelli, J. M. Guerreiro-Tanomaru, and M. Tanomaru-Filho, "Evaluation of Physicochemical Properties of Root-End Filling Materials Using Conventional and Micro-CT Tests," *Journal of Applied Oral Science* 25 (2017): 374–380.

38. F. M. Acris De Carvalho, Y. T. C. Silva-Sousa, C. E. Saraiva Miranda, et al., "Influence of Ultrasonic Activation on the Physicochemical Properties of Calcium Silicate-Based Cements," *International Journal of Dentistry* 7 (2021): 6697988.

39. I. M. Al-Sherbiny, M. H. Farid, A. M. Abu-Seida, I. T. Motawea, and H. A. Bastawy, "Chemico-Physical and Mechanical Evaluation of Three Calcium Silicate-Based Pulp Capping Materials," *Saudi Dental Journal* 33 (2021): 207–214.

40. M. Kaur, H. Singh, J. S. Dhillon, M. Batra, and M. Saini, "MTA Versus Biodentine: Review of Literature With a Comparative Analysis," *Journal of Clinical and Diagnostic Research* 11 (2017): 1–5.

41. B. M. Guimarães, C. Prati, M. A. H. Duarte, C. M. Bramante, and M. G. Gandolfi, "Physicochemical Properties of Calcium Silicate-Based Formulations MTA Repair HP and MTA Vitalcem," *Journal of Applied Oral Science* 5 (2018): e2017115.

42. A. L. Jalan, M. M. Warhadpande, and D. M. Dakshindas, "A Comparison of Human Dental Pulp Response to Calcium Hydroxide and Biodentine as Direct Pulp-Capping Agents," *Journal of Conservative Dentistry* 20 (2017): 129–133.

43. B. C. de Vasconcelos, R. A. Bernardes, S. M. Cruz, et al., "Evaluation of pH and Calcium Ion Release of New Root-End Filling Materials," *Oral Surgery, Oral Medicine, Oral Pathology, Oral Radiology, and Endodontics* 108 (2009): 135–139.

44. M. M. Almeida, C. T. Rodrigues, A. A. Matos, et al., "Analysis of the Physicochemical Properties, Cytotoxicity and Volumetric Changes of AH Plus, MTA Fillapex and TotalFill BC Sealer," *Journal of Clinical and Experimental Dentistry* 12 (2020): 1058–1065.

45. B. M. Guimarães, R. R. Vivan, B. Piazza, M. P. Alcalde, C. M. Bramante, and M. A. H. Duarte, "Chemical-Physical Properties and Apatite-Forming Ability of Mineral Trioxide Aggregate Flow," *Journal of Endodontics* 43 (2017): 1692–1696.

46. M. G. Gandolfi, P. Taddei, E. Modena, F. Siboni, and C. Prati, "Biointeractivity-Related Versus Chemi/Physisorption-Related Apatite Precursor-Forming Ability of Current Root End Filling Materials," *Journal of Biomedical Materials Research. Part B, Applied Biomaterials* 101 (2013): 1107–1123.

47. C. M. Silveira, S. C. Pinto, A. Zedebski Rde, F. A. Santos, and G. L. Pilatti, "Biocompatibility of Four Root Canal Sealers: A Histopathological Evaluation in Rat Subcutaneous Connective Tissue," *Brazilian Dental Journal* 22 (2011): 21–27.

48. M. G. Gandolfi, G. Iezzi, A. Piattelli, C. Prati, and A. Scarano, "Osteoinductive Potential and Bone-Bonding Ability of ProRoot MTA, MTA Plus and Biodentine in Rabbit Intramedullary Model: Microchemical Characterization and Histological Analysis," *Dental Materials* 33 (2017): 221–238.

49. T. Giraud, C. Jeanneau, C. Rombouts, H. Bakhtiar, P. Laurent, and I. About, "Pulp Capping Materials Modulate the Balance Between Inflammation and Regeneration," *Dental Materials* 35 (2019): 24–35.

50. B. Karabulut, N. Dönmez, C. C. Göret, C. Ataş, and Ö. Kuzu, "Reactions of Subcutaneous Connective Tissue to Mineral Trioxide Aggregate, Biodentine, and a Newly Developed BioACTIVE Base/Liner," *Scanning* 2020 (2020): 6570159.

51. A. Koutroulis, S. A. Kuehne, P. R. Cooper, and J. Camilleri, "The Role of Calcium Ion Release on Biocompatibility and Anti- Microbial Properties of Hydraulic Cements," *Scientific Reports* 9 (2019): 19019.

52. M. B. Queiroz, R. N. H. Inada, J. L. A. Jampani, et al., "Biocompatibility and Bioactive Potential of an Experimental Tricalcium Silicate-Based Cement in Comparison With Bio-C Repair and MTA Repair HP Materials," *International Endodontic Journal* 56 (2023): 259–277.